J Appl Electrochem (2011) 41:1407–1417
DOI 10.1007/s10800-011-0362-4

ORIGINAL PAPER

Time-efficient microwave synthesis of Pd nanoparticles and their electrocatalytic property in oxidation of formic acid and alcohols in alkaline media

S. K. Mehta · Sakshi Gupta

Received: 21 July 2011 / Accepted: 17 October 2011 / Published online: 1 November 2011

Abstract In this study time-efficient size controlled synthesis of stable Pd nanoparticles was carried out using microwave heating method by the decomposition of palladium chloride with glucose in aqueous medium using poly(ethyleneglycol) as capping agent. The benefit of the synthesis is that it was achieved in only 20 s. The synthesized Pd nanoparticles were characterized by UV–Visible spectroscopy, transmission electron microscopy, X-ray diffraction, and particle size analysis. The relative rates of electro-oxidation of formic acid, methanol and ethanol measured by cyclic voltammetry showed that efficiency of Pd nanoparticles as catalyst followed the order: formic acid < methanol < ethanol. The current–voltage characteristics improved with increase in either electrolyte (NaOH) or fuel concentrations but decreased with further increase in NaOH concentration.

Keywords Electro-oxidation · Cyclic voltammetry · Chronoamperometry · Diffusion controlled · Charge transfer plot

1 Introduction

The unique chemical, optical, electronic, and magnetic properties of metallic nanoparticles have led to a growing interest in their synthesis. Polymers control both the reduction rate of metal ions and the aggregation process of metal atoms. Preparation of polymer-stabilized nanoparticles by a chemical method involves two processes: reduction of metal ions to zero valent atoms and coordination of the stabilizing polymer to metal nanoparticles. Figure 1 illustrates a typical stabilization structure of a metal nanoparticle by soluble polymers in an aqueous solution [1]. Stabilizing polymers can be adsorbed on the surface of hydrophobic metal nanoparticles. Hydrophobic "train" segments can be directly adsorbed on the surface of solid metal, and hydrophilic "loop" or "tail" segments spread out into the hydrophilic solvent. Many studies [2, 3] have focused on improving methods for size-controlled synthesis of metal nanoparticles, however, there is still a significant challenge in obtaining a targeted nanoparticle size from a given set of synthetic conditions due to difficulties in avoiding formation of new nucleation sites during the growth stage.

Pd is an important transition metal with high catalytic activity [4, 5], although it has not been used as widely as Pt [6]. Recently, much attention has been focused on the preparation of Pd nanoparticles and their application in the fields of catalysis [7], hydrogen storage [8], and chemical sensors [9] because of the large surface area-to-volume ratio, relatively lower price than Pt, and especially the unique function in absorption of hydrogen [10, 11]. Pd exhibits interestingly much higher catalytic activity than Pt toward formic acid electro-oxidation, since it is free from poisoning by CO [12, 13]. In acidic solutions, Pd catalysts possess low catalytic activity for the oxidation of small organic molecules except formic acid; however, they show very high catalytic activity in alkaline solutions [14, 15].

Polyethyleneglycol (PEG) has been widely used as stabilizer in the synthesis of Pd nanoparticles [16–19]. Namini et al. [20] have synthesized Pd nanoparticles with narrow size distribution by loading metal salt ($Pd(OAc)_2$) into the polymeric matrix, PEG as both reducing agent and stabilizer. Although PEG was only used as reducing agent and stabilizer, the method was however time consuming.

S. K. Mehta (✉) · S. Gupta
Department of Chemistry & Centre of Advanced Studies in Chemistry, Panjab University, Chandigarh 160 014, India
e-mail: skmehta@pu.ac.in

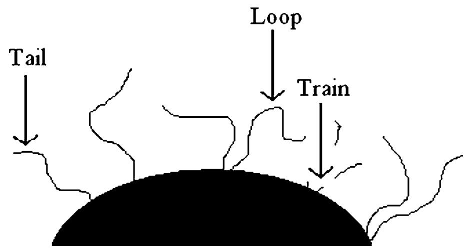

Fig. 1 Schematic representation of stabilizing structure of polymers on the surface of metal nanoparticles

Mallikarjuna and Varma [21] described bulk and shape-controlled syntheses of Pd nanostructures through microwave (MW) reduction of noble metal salts using an aqueous solution of α-D-glucose, sucrose and maltose using poly(vinylpyrrolidinone) in 30–60 s. MW dielectric heating is a new promising technique for the preparation of size-controlled metallic nanoparticles due to rapid heating and penetration. In comparison with conventional heating, this method can shorten the reaction time by a factor of approximately 20. In addition, heating is not only quick but also uniformly spread over the entire volume of the reaction mixture as it provides rapid and uniform heating of reagents, solvents, and intermediates [22, 23]. Currently, there is a growing need to develop such ecofriendly processes that avoid the use of toxic chemicals in the preparative protocol with increased emphasis on the synthesis of nanoparticles using greener methods. Glaspell et al. [24–27] have reported the synthesis of unsupported and oxide supported Pd nanoparticles synthesis through microwave and other methods and their use in catalysis. Many authors [28–30] have also investigated on the synthesis of supported Pd as nanocatalysts. In a recent report, Ravishankar and coworkers [31] have described the selective heterogeneous nucleation of metal nanoparticles on oxides by microwave-assisted reduction and their activity as supported catalysts. However our method is superior to others in terms of rapid generation and stabilization of Pd nanoparticles in water with a cheap, readily available PEG and glucose. The size of the nanoparticles generated can be controlled by the concentration of reagents in water medium. Nanoparticle catalysis in water has an advantage of carrying out efficient reactions under environmentally benign conditions associated with green chemistry.

In an attempt to develop greener methods to synthesize noble nanostructures, in this article we report an environmentally benign approach that provides easy production of nanostructures. Pd nanoparticles with narrow size distribution have been synthesized by exploiting α-D-glucose as reducing agent and PEG as stabilizer in 20 s, by heating in MW. In addition to the MW irradiation time,the effects of Pd nanoparticles morphology, polymeric matrix PEG, and glucose concentration effects on the conversion of Pd^{2+} to nano Pd^0 have been analyzed using UV–Vis spectroscopy, transmission electron microscopy (TEM), X-ray diffraction (XRD), and particle size analysis (PSA) techniques. To the best of our knowledge, there has not been any prior study of synthesis of Pd nanoparticles in just 20 s, despite the current interest in its application in direct fuel cells. In addition, the synthesized nanoparticles have been employed in catalysis of reactions such as electro-oxidation of formic acid, methanol and ethanol using cyclic voltammetry (CV).

2 Materials and methods

All reagents were of the highest purity. PEG (Molecular weight 20,000) and methanol (>99%) were purchased from Merck. Palladium (II) chloride ($PdCl_2$) (99%) was obtained from Aldrich. α-D-glucose (99.5%) was purchased from Hi Media. Formic acid (98–100%) and ethanol (99.9%) were obtained from BDH and Changshu Yangyuan (China), respectively. All these chemicals were used without further purification. Freshly deionized and distilled water (conductivity = 3–4 μS) was used as dispersion medium throughout the experiments.

2.1 Preparation of PEG stabilized Pd nanoparticles

Solutions were prepared freshly to avoid photochemical reactions. All experiments were carried out in air. Monometallic Pd nanoparticles were synthesized using $PdCl_2$ as precursor, α-D-glucose as reducing agent and PEG as stabilizer. 5 mM solution of $PdCl_2$ was prepared using double distilled water. Required amounts of glucose and PEG were added to the solution. It was heated in domestic MW oven for 20 s. The light brown colour changed to blackish brown indicating the formation of Pd nanoparticles, and the particles were stable for months at room temperature.

2.2 Characterizations

Experiments were carried out in domestic MW oven (IFB-20PG2S, power supply 230 V/50 Hz, consumption 1,200 W, output power 800 W, and operation frequency 2,450 MHz) at 60% power. UV–Vis spectroscopic measurements were performed on a Thermo Fisher Scientific Evolution 160 UV–Vis spectrophotometer at room temperature using 1 cm quartz cuvettes. The PEG coated Pd nanoparticles were characterized by TEM at 80 kV with a Hitachi H-7500 electron microscope. The selected area electron diffraction (SAED) was also recorded. Samples for TEM and SAED were prepared by placing a drop of the colloidal dispersion of PEG–Pd nanoparticles onto a gold grid, and the solvent was allowed to evaporate naturally. The sample for XRD was prepared by the same procedure followed by washing first by water and then by acetone to remove all the unreacted material. It was dried in air to get solid sample. The XRD patterns were determined on a Panalytical's X'Pert Pro X-ray Diffractometer (Powder method) using CuKα as radiation ($\lambda = 1.54$ Å). Data were collected in the range $5 \leq 2\theta° \leq 80$ with a 0.02° 2θ-step. PSA analysis was performed using Malvern Zetasizer nanoseries.

2.3 Electrochemical studies

Electrochemical measurements were performed using a μAutolab Type-III cyclic voltammeter using conventional three-electrode cell, which includes an Ag/AgCl electrode (saturated KCl) as reference electrode, a Pt wire as counter electrode, and a glassy carbon (GC) electrode (2 mm in diameter) as working electrode. The GC electrode was first carefully polished with fine alumina powder and a certain amount of required solution was pipetted onto the GC electrode and allowed to dry under an infrared lamp. The CV and chronoamperometry (CA) experiments were carried out in 0.5 M NaOH (Qualigens) individually when the scan rate was 0.1 Vs^{-1}, for catalysing 0.5 M formic acid, methanol and ethanol.

3 Results and discussion

3.1 UV–Vis spectroscopic studies

To prepare the stable Pd nanoparticles using the chemical reduction method, it is important to select appropriate stabilizer and reducing agent. In present work, $PdCl_2$ has been reduced by glucose in the presence of stabilizer PEG, resulting in Pd nanoparticles, according to the Eq. (1).

$$Pd^{2+} + CH_2OH{-}(CHOH)_4{-}CHO + H_2O \xrightarrow{MW,20S} Pd^0 + 2H^+ + CH_2OH{-}(CHOH)_4{-}COOH \quad (1)$$

The nanoparticles have been synthesized at the conditions of constant amounts of $PdCl_2$, glucose and PEG. The colour of the solution depends on the heating time. UV–Vis spectra of colloidal Pd nanoparticles prepared with different MW heating time (5, 10, 15, 20 s) have been depicted in Fig. 2a. With increasing time, the colour of solution changed from light brown to blackish brown and absorbance also increased till 20 s. However, on further microwaving, no change in absorbance was observed even after 20 s up to 30 s which indicated that the reaction has been completed in 20 s. Mallikarjuna and Varma [21] reported the synthesis of Pd nanoparticles along with other metals in 30–60 s whereas Pd nanoparticles in the present system has been synthesized in 20 s only. It has been observed that the absorbance increases in the presence of both glucose and PEG (Fig. 2b). Thus, both PEG and glucose increase the efficiency of the reduction of Pd precursor.

To understand the role of glucose concentration, the reduction reaction has been carried out by varying concentration of glucose (50–400 mg) at the conditions of initial $PdCl_2$ concentration (5 mM) and PEG (300 mg). UV–Vis spectra of different amounts of glucose have been shown in Fig. 2c. With small amount of glucose, a weak

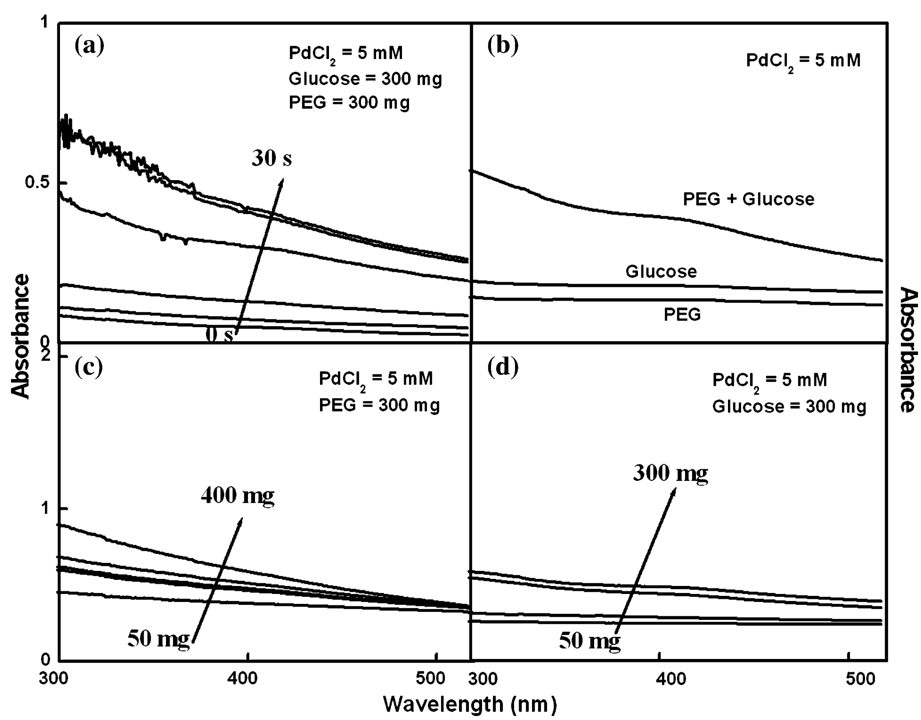

Fig. 2 UV-Vis absorption spectra showing effects of **a** increasing MW heating time, **b** both PEG and glucose, **c** increasing concentration of glucose and **d** increasing concentration of PEG

absorption has been observed, indicating that Pd nanoparticles of a relatively low concentration were produced, because of insufficient reduction reaction. The main purpose of introducing PEG to the solution was to prevent the Pd nanoparticles from growth and aggregation. Figure 2d depicts the UV–Vis spectra of colloidal Pd nanoparticles with different PEG concentrations (50–300 mg). The nanoparticles were synthesized at the conditions of initial $PdCl_2$ (5 mM) and glucose concentration (300 mg). When adequate amount of PEG was used, it adsorbs on the surface of Pd nanoparticles, and protects nanoparticles from growth and aggregation because of its steric effect.

3.2 TEM studies

Figure 3 shows the TEM images of Pd nanoparticles prepared with different glucose and PEG amounts. The nanoparticles synthesized have shown fair monodispersity. The particles are nearly spherical in shape. With increasing the glucose concentrations, the particle size changes have been observed (Fig. 3a–c). The size variations with change in amounts of glucose and PEG estimated from TEM and PSA have been shown in Table 1. The size variation may be because, with an increase in the concentration of the reducing agent, the reduction rate of metal ions increases, leading to smaller metal nanoparticles.

The TEM image (Fig. 3d) of the sample synthesized from 100 mg PEG and 300 mg glucose showed aggregation of the particles which concluded that 100 mg PEG was insufficient for capping the nanoparticles. While, the amount of PEG was increased (Fig. 3c, e), monodisperse particles were seen. No aggregates were observed in other samples, and the nanoparticles prepared showed good size distribution.

Table 1 Size of the nanoparticles observed from TEM images

TEM image	Glucose (mg)	PEG (mg)	Approximate size (nm)	
			TEM	PSA
3(a)	100	300	30	37.8
3(b)	200	300	15	21.0
3(c)	300	300	10	7.5
3(d)	300	100	Aggregate	–
3(e)	300	400	12	18.1

3.3 XRD and PSA studies

Figure 4a shows the XRD pattern of the particles. The characteristic peaks for Pd ($2\theta = 40.1$, 46.7,and 67.9), marked by their indices ((111), (200), and (220)), reveal face-centered cubic (fcc) structure of Pd particles. Extra noise can be because of PEG. The crystallite size was estimated by applying the Scherrer equation (Eq. 2) to the full width at half maxima (FWHM) of the (111) peak of Pd nanoparticles:

$$\tau = \frac{K\lambda}{\beta \cos \theta} \tag{2}$$

where K is the shape factor (0.94 for spherical shapes), λ is the X-ray wavelength, typically 1.54 Å, β is the FWHM,

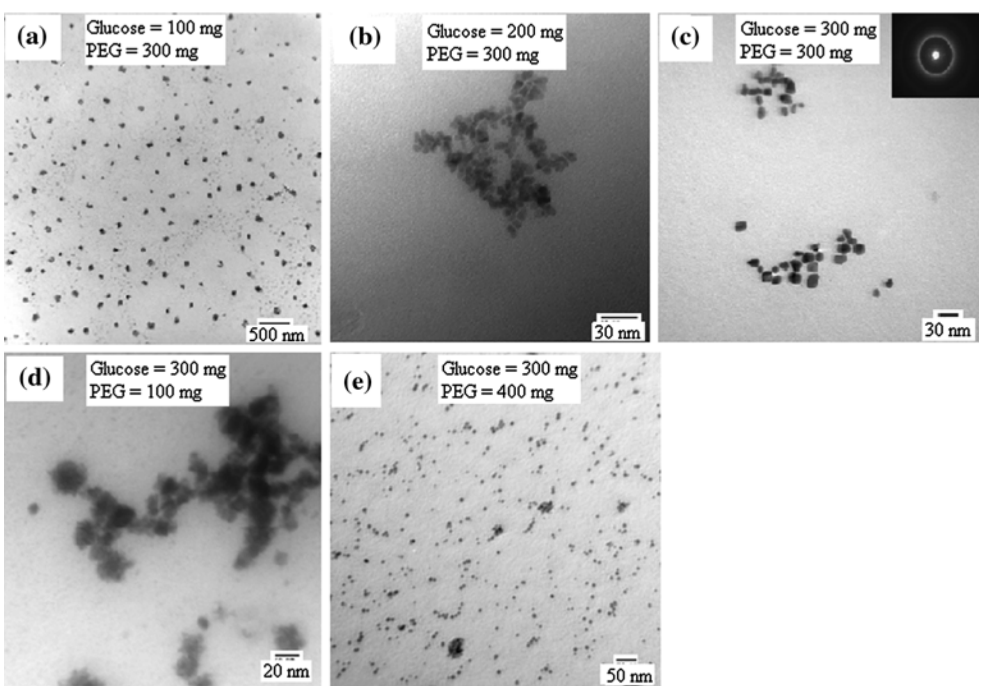

Fig. 3 TEM images of Pd nanoparticles obtained by changing the concentrations of glucose and PEG

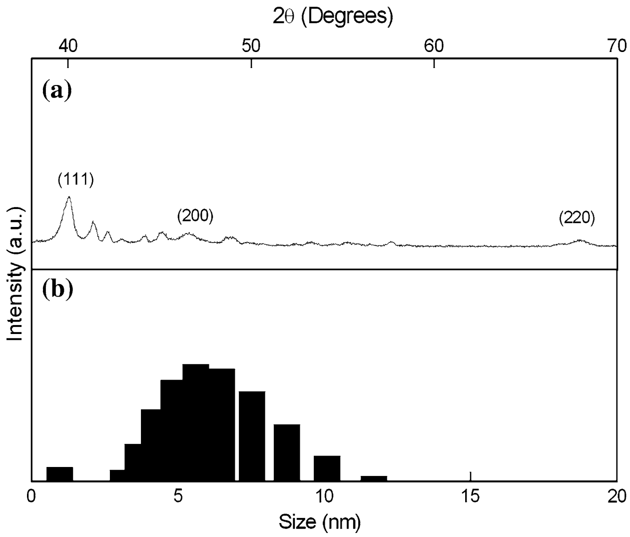

Fig. 4 **a** XRD pattern of Pd nanoparticles synthesized in MW. **b** Size distribution histogram obtained from PSA

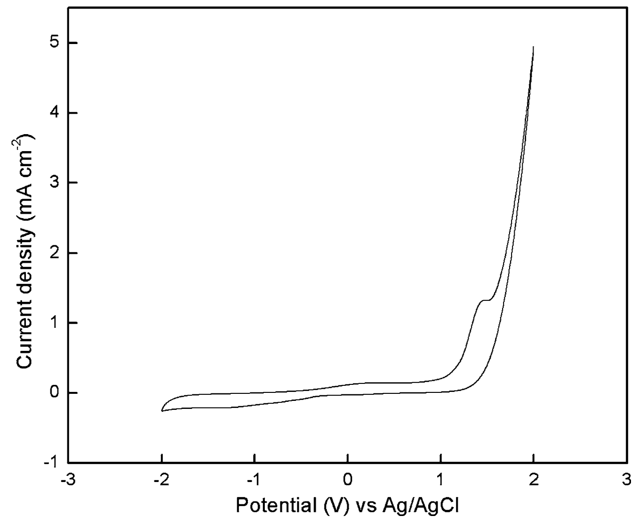

Fig. 5 CV of the Pd nanoparticles modified GC electrode in 0.5 M NaOH solution at 0.1 Vs^{-1}

θ is the Bragg angle in radians, and τ is the mean size (nm) of the particle. The XRD data yield particle size of 10.6 nm when using 300 mg glucose, which is in good agreement with the average size of 10 nm as obtained from TEM data. The PSA (Fig. 4b) also shows that the nanoparticles synthesized are of mean diameter of approx. 7.5 nm.

3.4 Electrocatalytic studies

3.4.1 Electro-oxidation of fuels

With the development of nanotechnology, nanostructures provide more opportunities for searching or designing an effective catalyst for such materials. Recently [32–34], Pd-based electrocatalysts, as one of the non-Pt electrocatalysts, have been found to possess prominent properties for catalyzing alcohol or formic acid. Fig. 5 depicts the CV of the Pd nanoparticles modified GC electrode in 0.5 M NaOH solution in the absence of any organic compound. By comparing to the CV in the absence of fuel, an oxidation peak of the fuel can be clearly observed.

The most active catalyst for the formic acid oxidation is made of the smallest Pd nanoparticles [35]. Such small Pd nanoparticles display the highest binding energy shift and the highest valence band center downshift with respect to the Fermi level [35]. In other words, the smallest nanoparticles display the highest formic acid reactivity. For formic acid oxidation to CO_2, the mechanism can be summarized as follows:

$$(HCOOH)_{ads} \rightarrow (COOH)_{ads} + H^+ + e^- \quad (3)$$

$$(COOH)_{ads} \rightarrow (CO_2)_{rds} + H^+ + e^- \quad (4)$$

The rate of formic acid transformation to CO_2 (Eq. 3) is the highest at the surface. Since the smallest Pd nanoparticles have the lowest *d*-band center, they bind the COOH intermediate less strongly (versus larger nanoparticles) and reduce the surface $(COOH)_{ads}$ coverage (Eq. 4). If the limiting step, i.e., Eq. 4 is avoided because of the low COOH coverage, then higher rates of the direct HCOOH decomposition process to CO_2 are expected.

Keeping in view that smallest nanoparticles of Pd act as active catalyst, in the present study, we have used 10 nm size Pd nanoparticles in the electro-oxidation. Figure 6a is the CV scan of formic acid electro-oxidation in 0.5 M NaOH containing 0.5 M formic acid on different materials modified GC electrodes at the scan rate of 0.1 Vs^{-1}. There is an oxidation peak at about 0.063 V (versus Ag/AgCl) in the forward scan, which is ascribed to the electro-oxidation of formic acid, and another oxidation peak in the reverse scan mainly corresponds to the residual carbon fuels formed in the forward scan. The unexpected steep slopes in CV are due to fast mass transport in diffusion process. Bravo et al. [36] investigated the determination of amount of uric acid with the help of carbon fiber electrode. They reported that the steep rise of the current–potential curve of uric acid points to fast electrode kinetics of uric acid at carbon fiber electrode surface. Similarly, Toth et al. [37] also reported that steep angles in CV are due to the fast kinetics on the electrode due to fast mass transport.

Similarly, for methanol oxidation, the following reactions have been observed [38]:

$$(CH_3OH)_{ads} \rightarrow (CHO)_{ads} + 3H^+ + 3e^- \quad (5)$$

$$(CHO)_{ads} + OH^- \rightarrow (HCOOH)_{ads} + e^- \quad (6)$$

$$(HCOOH)_{ads} \rightarrow (COOH)_{ads} + H^+ + e^- \tag{7}$$

$$(COOH)_{ads} \rightarrow (CO_2)_{rds} + H^+ + e^- \tag{8}$$

The CV scan of methanol electro-oxidation with modified GC electrode under same conditions as above has been presented in Fig. 6b. It shows the oxidation peak at about −0.159 V (versus Ag/AgCl) in the forward scan.

Besides the above, ethanol electro-oxidation has received increasing attention since ethanol is less toxic than methanol and can be easily produced in great quantity by the fermentation of sugar-containing raw materials. The Pd-based catalyst used for ethanol electro-oxidation in alkaline media has been developed recently. There is a generally accepted reaction scheme for ethanol oxidation on Pt-based catalysts. The reaction mechanism [39] is actually split into three paths leading to either acetaldehyde or acetic acid formation, and a path leading to CO_2 formation. For each path, however, the low-potential activation of water by the electrocatalyst (Eqs. 9 and 10) is mandatory to accomplish both the oxidation of CO_{ads} to CO_2 and the C–O coupling that transforms $acyl_{ads}$ into acetic acid:

$$(OH_2)_{ads} \rightarrow (OH)_{ads} + H^+ + e^- \tag{9}$$

$$(OH)_{ads} \rightarrow (O)_{ads} + H^+ + e^- \tag{10}$$

$$(CO)_{ads} + (O)_{ads} \rightarrow CO_2 \tag{11}$$

The surface structure sensitivity of ethanol oxidation is due in part to facile C–C bond cleavage at step sites. The faster C–C bond breaking kinetics lead to larger CO_2 yields [40], but it occurs at the expense of increased poisoning by adsorbed CO and possibly other partial oxidation products. The decrease in acetic acid production is likely a consequence of (i) a shift in reactions toward the CO_2 producing pathway and (ii) increased surface poisoning that blocks sites for water activation. The CV scan of ethanol electro-oxidation with modified GC electrode under same conditions as for formic acid and methanol (Fig. 6c) shows the oxidation peak at about −0.180 V (versus Ag/AgCl) in the forward scan. The results indicates that it possesses better electrocatalytic behavior than Pd nanoparticles used by Liu et al. [41] and bulk Pd employed by Zhou et al. [42]. The oxidation peaks of the fuels in Fig. 5 are consistent with the recent results [43, 44] [Table 2]. The similar results confirm that the peaks are due to the oxidation of the fuels being oxidized. Bambagioni [44] reported the oxidation potentials of methanol and ethanol as −0.15 and −0.12 V (versus Ag/AgCl) on a Pd/MWCNT electrode.

The intermediate carbonaceous fuels formed during electro-oxidation may poison the catalyst and suppress its performance accordingly. Therefore, the stability of the synthesized Pd nanoparticles for electro-oxidation was investigated by multicycles in CV and CA [45]. Figure. 6d–f shows the cyclic voltammograms of electro-oxidation in 0.5 M NaOH at a scan rate of 0.1 Vs^{-1}. The peak current density of formic acid during the first cycle has been 5.697 mA cm^{-2} as compared to 5.090 mA cm^{-2} in the fifteenth cycle, which is just 10.06% less than that during the first scan. Similarly, the efficiency has also been calculated for the other two. The peak current densities for

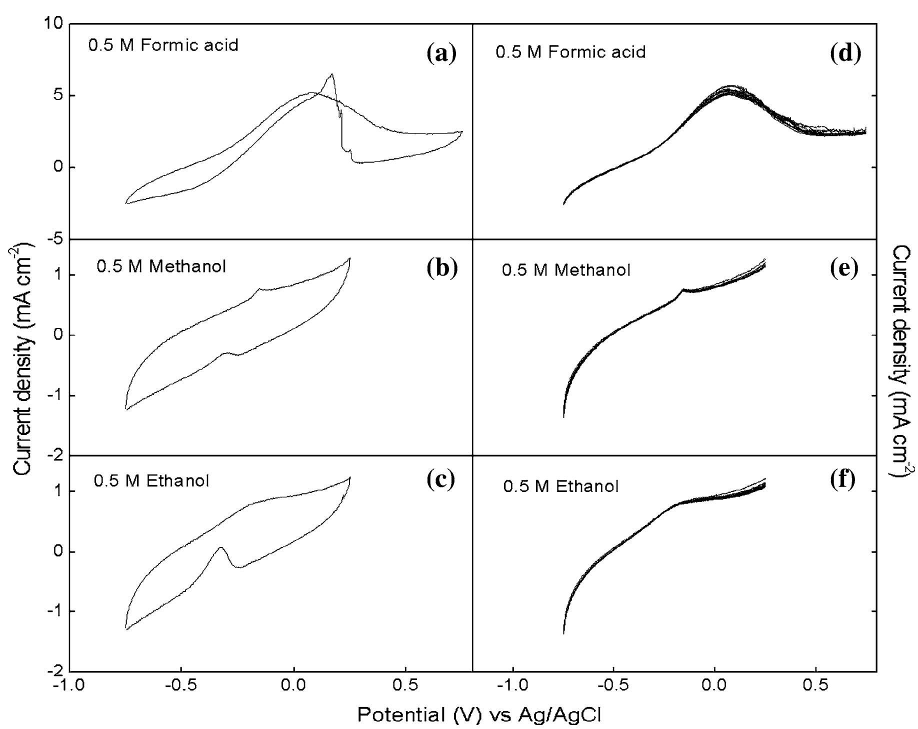

Fig. 6 (**a**–**c**) CV scans of oxidation on Pd (10 nm) unsupported catalyst in 0.5 M NaOH solution at 0.1 Vs^{-1} scan rate and (**d**–**f**) forward CV scans of oxidation for 15 cycles

Table 2 The oxidation peaks and I_f/I_b ratios of the fuels with the references have been reported with the comparable peaks

Fuel	Oxidation potential observed* (V)	Reference	I_f/I_b ratio
Formic acid	0.063	43	0.792
Methanol	−0.159	44	2.640
Ethanol	−0.180	44	15.674

*(V versus Ag/AgCl)

fifteenth cycle have been 1.99 and 1.72% less than the first scan for methanol and ethanol, respectively. The efficiency of the synthesized Pd nanoparticles for electro-oxidation of methanol and ethanol has been found to be very high.

The ratio of the forward oxidation current peak (I_f) to the reverse current peak (I_b), i.e., I_f/I_b, is an index of the catalyst tolerance to the poisoning fuels [46]. A higher ratio indicates more effective removal of the poisoning fuels from the catalyst surface. The I_f/I_b ratios (Table 2) follows the order: formic acid < methanol < ethanol, which indicates that Pd nanoparticles of size ~10 nm act as better catalysts for ethanol compared to other two. The activation energy of ethanol is low; therefore, ethanol gets more easily electrochemically oxidized than methanol [47].

3.5 Chronoamperometric studies

In a CA experiment, the potential is held constant, and the resulting current transient is measured [48]. Figure 7a, c, and e shows the current-time plots for 1 h of 0.5 M formic acid, methanol, and, ethanol, respectively, in 0.5 M NaOH. In all the cases, the Pd catalyst shows good performance in electro-oxidation. All the transients display appreciable current during the early stages of oxidation. Figure 7a shows very pronounced digital noise in CA tests. It may be due to the CO poisoning of the catalyst which is also contributing to the low efficiency of the nanoparticles toward oxidation of formic acid. Recently, Winjobi and coworkers [49] have employed carbon nanotube supported Pt–Pd nanoparticles for formic acid oxidation. They have also reported that unclear chronoamperograms, which is again because of the CO_{ads} poisons that gradually accumulate on the catalyst surface and deteriorate the catalyst activity.

Further CA plots have been employed in calculating the charge transfer plots [50] in each case (Fig. 7b, d, f).From the plots also we infer that the oxidation is linear, i.e., uniform. This means that the Pd nanoparticle of size 10 nm shows superior catalytic activity in electro-oxidation of alcohols and good catalytic activity in electro-oxidation of formic acid.

The CV scans of Pd nanoparticles (10 nm) in formic acid, methanol, and ethanol in 0.5 M NaOH solution have also been carried at various scan rates v: 0.07−0.5 Vs^{-1}. A linear relationship is found between the oxidation peak current and $(v)^{1/2}$, as shown in Fig. 8, indicating that the oxidation can be a diffusion-controlled process [51]. The electro-active area of the nanoparticles modified GC electrode is determined by the plot of i_p against $v^{1/2}$ (Fig. 8a) using the following Randles–Sevcik equation [52]:

$$i_p = \left(2.69 \times 10^5\right) n^{3/2} A\, D^{1/2}\, v^{1/2}\, C \tag{12}$$

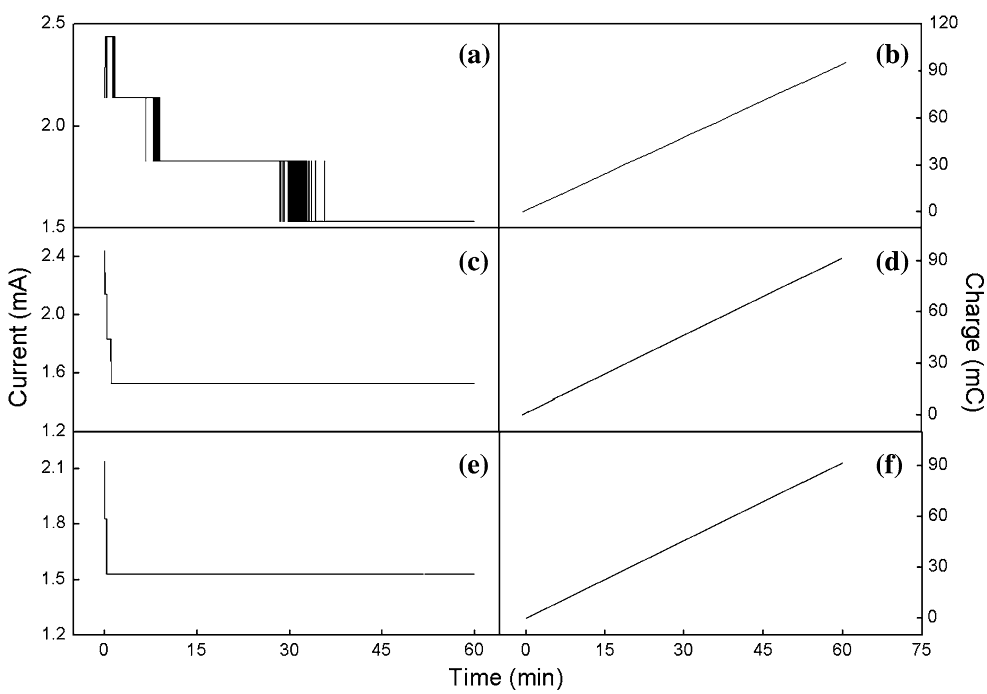

Fig. 7 CA current-time plots for 1 h in 0.5 M NaOH and charge transfer plots (**a**, **b**) 0.5 M Formic acid, (**c**, **d**) 0.5 M Methanol, (**e**, **f**) 0.5 M Ethanol

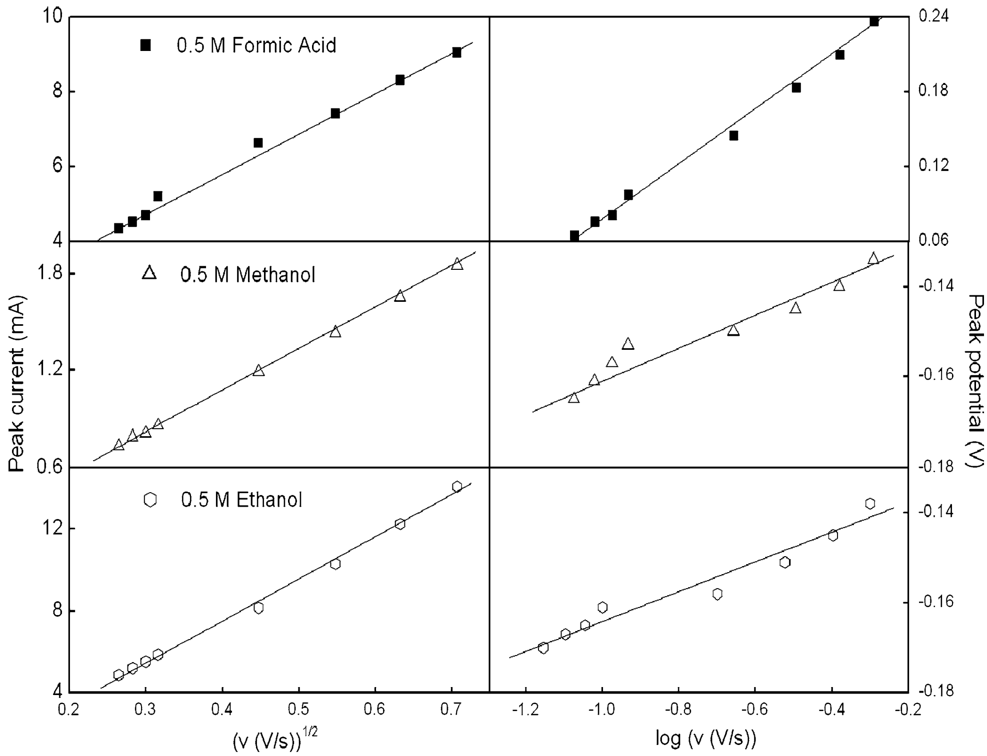

Fig. 8 Variations of peak current and peak potential as a function of different scan rates on Pd nanoparticles (10 nm) in 0.5 M NaOH

For formic acid, $n = 2$ (Eqs. 3 and 4), A is the electroactive area of the nanoparticles modified GC electrode, v is the potential scan rate, and C is the concentration of formic acid in 0.5 M NaOH, and D is the diffusion coefficient of formic acid. The electroactive area calculated for synthesized Pd nanoparticles is 74.119 mm^2.

In addition, the peak potential (E_p) increases with the increase in v and a linear relationship is obtained between E_p and log v. The results show that the oxidation on the Pd nanoparticles is an irreversible process [51].

3.5.1 *Effect of concentrations of fuels and electrolyte*

The peak current density is affected by both fuel and NaOH concentrations [45]. Figure 9a–c shows the effect of concentration of the fuels to be oxidized on electro-oxidation in alkaline medium. NaOH concentration has been maintained at 0.5 M, and the fuel concentration has been varied. The anodic peak current density during the forward scans increases with the increase in concentrations examined. Therefore, the electro-oxidation is concentration-dependent, and the anodic current density is proportional to the concentration of the fuel to be oxidized and is not yet saturated under the investigated fuel concentration range. In addition, a positive shift in peak potential is observed as fuel concentration increases.

Figure 9d–f depicts the effect of NaOH concentration on electro-oxidation by fixing the fuels' concentrations at 0.5 M and varying NaOH concentration. The anodic peak current density in the case of formic acid increases with the increase in NaOH concentration initially and then reaches a maximum value at 0.5 M NaOH. Further increase of NaOH concentration has an inverse effect on the current density. Initial increase of NaOH concentration could have greatly facilitated the adsorption of the hydroxide ion as well as formic acid to be oxidized on Pd active sites. However, when the NaOH concentration is too high, there is no sufficient active site on the Pd surface, and further increase of NaOH concentration results in the adsorption of OH^- being dominant. There might be no difference between the active sites for the formic acid and OH^- on the surface of Pd, and their adsorptions follow a competitive mechanism when the available active sites are insufficient. Therefore, there is a net decrease in the active sites for formic acid. Similar explanation is applicable for both methanol and ethanol cases, where maximum value for NaOH is 0.8 M.

Figure 10 shows the plots between the ratio of NaOH concentration and fuel to be oxidized and the peak potential for all systems. In all the cases, there is a particular ratio of the concentrations after which the equation changes. There seems to be a correlation between the peak potential and the ratio of NaOH concentration and the fuel

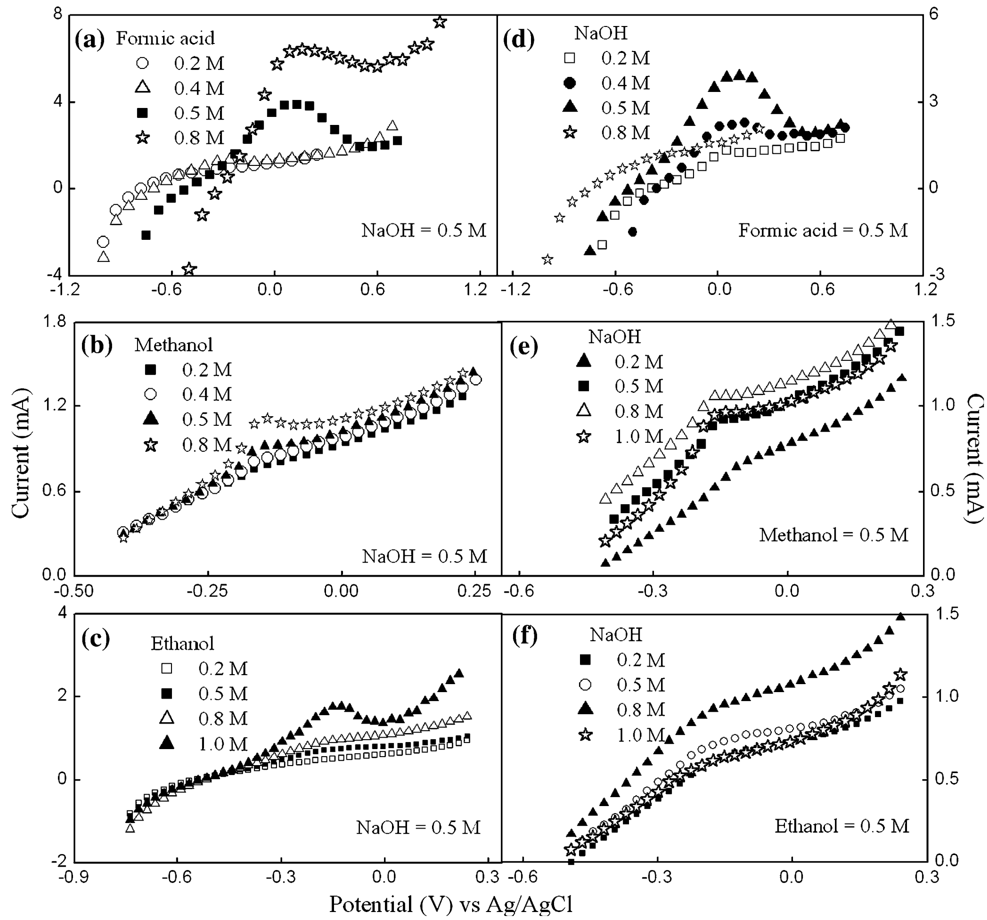

Fig. 9 Effect of concentration on the forward CV scans using Pd (10 nm) unsupported catalyst at a scan rate of 0.1 Vs^{-1}

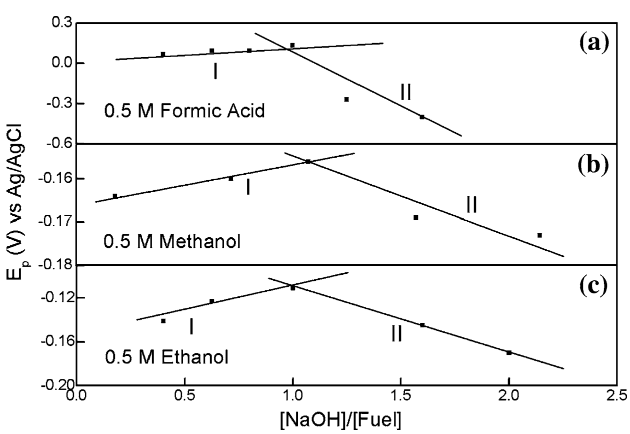

Fig. 10 The change in peak potential with the ratio of NaOH concentration to fuel concentration where Fuel = Formic acid or methanol or ethanol

to be oxidized. Table 3 lists the regression and the peak potential equation of all the plots. The linear regression constants (R^2) have been found to be good. The data support that the ratio instead of any one of the concentration alone is the determinant factor for the shift of peak potential on the as-prepared Pd nanoparticles.

Table 3 Linear regression constants and E_p equations for different fuels

Fuels	Line*	R^2	E_p (V)
Formic acid	I	0.8953	+0.0993 (ratio) + 0.0271
	II	0.8613	−0.8553 (ratio) + 0.9190
Methanol	I	0.9868	−0.0126 (ratio) − 0.1721
	II	0.8911	−0.0224 (ratio) − 0.1298
Ethanol	I	0.9347	−0.0482 (ratio) − 0.1575
	II	0.9992	−0.0588 (ratio) – 0.0518

*In fig. 10

In summary, well-defined forward and backward scan peaks have been observed for formic acid, methanol, and ethanol, which indicate the good electrocatalytic activity of the synthesized Pd nanoparticles for the electro-oxidation. The prepared Pd nanoparticles (10 nm) have produced stable and reproducible response to oxidation of formic acid, methanol, and ethanol. The enhanced performance may be attributed to the large surface area, reduced diffusion resistance, good catalytic ability, and excellent poisoning tolerance of the nanoparticles catalyst. Thus, the free-standing Pd nanoparticles have great potential applications in various direct alcohol fuel cells.

4 Conclusions

Nanostructures of noble metal, i.e., Pd with varying sizes have been generated from aqueous glucose solutions using MW irradiation. The synthesis has been done in few seconds, i.e., 20 s along with the control in the size of nanoparticles. Specifically, bulk and size-controlled synthesis of nanostructures of Pd with particle size from 10 to 30 nm have been achieved depending upon the concentration of sugar solution. The role of concentration of the metal ion, reducing agent, and capping polymer to prepare smaller nanoparticles has been explored through UV–Visible spectroscopic studies. These nanoparticles are highly stable in aqueous solution, and the stabilization results from the adsorption of the long PEG chain on the particle surface through the interaction of the PEG groups with the Pd surface. By combining several characterizations, such as UV–Vis spectroscopy, TEM, XRD, and PSA, the product is proved to possess size in the order nanoscale. TEM results reveal that the glucose concentration has significant effect on the size of the synthesized Pd nanoparticles. It is also documented here that Pd nanoparticles exhibit good activity for the electro-oxidation of formic acid and alcohols in alkaline solutions. The nanoparticles are highly efficient for the electro-oxidation of alcohols. The electro-oxidation peaks of formic acid, methanol and ethanol can be easily described by cyclic voltammograms, current–time plots and charge transfer plots. It is proved that electro-oxidation is diffusion controlled and irreversible and the prepared Pd nanoparticles are quite stable as catalysts. The electro-oxidation is also concentration dependent as it depends on the concentrations of electrolyte as well as the fuel used in the system. The experiments on formic acid, methanol, and ethanol oxidation reveal that the prominent catalytic properties can promote this new electrocatalyst, i.e., PEG coated nanoparticles to be applicable in fuel cells.

Acknowledgments SKM and Sakshi Gupta are thankful to the Department of Science and Technology (DST) and the Council of Scientific & Industrial Research (CSIR), India for the financial assistance and fellowship.

References

1. Toshima N, Yonezawa T (1998) New J Chem 22:1179
2. Liu J, Sutton J, Roberts CB (2007) J Phys Chem C 111:11566
3. Collier CP, Saykally RJ, Shiang JJ, Henrichs SE, Heath JR (1997) Science 277:1978
4. Baldauf M, Kolb DM (1993) Electrochim Acta 38:2145
5. Hoshi N, Kida K, Nakamura M, Nakada M, Osada K (2006) J Phys Chem B 110:12480
6. Baldauf M, Kolb DM (1996) J Phys Chem 100:11375
7. Niwa O, Kato D, Kurita R, You T, Iwasaki Y, Hirono S (2007) Sens Mater 19:225
8. Rose A, Maniguet S, Mathew RJ, Slater C, Yao J, Russell AE (2003) Phys Chem Chem Phys. 5:3220
9. Sun Y, Wang HH (2007) Appl Phys Lett. 90:213107
10. Czerwinski A, Kiersztyn I, Grden M, Czapla J (1999) J Electroanal Chem 471:190
11. Grden M, Piascik A, Koczorowski Z, Czerwinski A (2002) J Electroanal Chem 532:35
12. Miyake H, Okada T, Samjeske G, Osawa M (2008) Phys Chem Chem Phys 10:3662
13. Rice C, Ha S, Masel RI, Wieckowski A (2003) J Power Sources 115:229
14. Su YZ, Xu CW, Liu JP, Liu ZQ (2009) J Power Sources 194:295
15. Liang ZX, Zhao TS, Xu JB, Zhu LD (2009) Electrochim Acta 54:2203
16. Huang TS, Wang YH, Jiang JY, Jin ZL (2008) Chin Chem Lett. 19:102
17. Feng B, Hou Z, Yang H, Wang X, Hu Y, Li H, Qiao Y, Zhao X, Huang Q (2010) Langmuir 26:2505
18. Uozumi Y, Nakao R, Rhee HJ (2007) Organomet Chem 692:420
19. Hou ZS, Theyssen N, Brinkmann A, Leitner W (2005) Angew Chem Int Ed 44:1346
20. Namini PA, Babaluo AA, Bayati B (2007) Int J Nanosci Nanotech 3:37
21. Mallikarjuna NN, Varma RS (2007) Cryst Growth Des 7:686
22. Varma RS (2006) Kirk-Othmer Encycl Chem Tech 16:538
23. Polshettiwar V, Varma RS (2008) Acc Chem Res 41:629
24. Yang Y, Saoud KM, Abdelsayed V, Glaspell G, Deevi S, El-Shall MS (2006) Catal Commun 7:281
25. Glaspell G, Fuoco L, El-Shall MS (2005) J Phys Chem B 109:17350
26. Glaspell G, Hassan H, Fuoco L, El-Shall MS (2006) J Phys Chem B 110:21387
27. Glaspell G, Hassan HMA, Elzatahry A, Abdalsayed V, El-Shall MS (2008) Top Catal 47:22
28. Hu F, Cui G, Wei Z, Shen PK (2008) Electrochem Commun 10:1303
29. Gopinath R, Rao KN, Prasad PSS, Madhavendra SS, Narayanan S, Vivekanandan G (2002) J Mol Catal A 181:215
30. Shironita S, Takasaki T, Kamegawa T, Mori K, Yamashita H (2009) J Phys: Conf Ser 165:012039
31. Anumol EA, Kundu P, Deshpande PA, Madras G, Ravishankar N (2011) ACS Nano doi:10.1021/nn202639f
32. Rhee Y-W, Ha SY, Masel RI (2003) J Power Sources 117:35
33. Bath BD, White HS, Scott ER (2000) Anal Chem 72:433
34. Song SQ, Tsiakaras P (2006) Appl Catal B 63:187
35. Zhou W, Lee JY (2008) J Phys Chem C 112:3789
36. Bravo R, Hsueh CC, Brajter-Toth A, Jaramillo A (1998) Analyst 123:1625
37. Brajter-Toth A, El-Nour KA, Cavalheiro ET, Bravo R (2000) Anal Chem 72:1576
38. Bagotzky VS, Vassiliev YB, Khazora OA (1977) J Electroanal Chem 81:229
39. Hao E, Scott K (2004) J Power Sources 137:248
40. Leung LWH, Chang SC, Weaver MJ (1989) J Electroanal Chem 266:317
41. Liu Z, Zhao B, Guo C, Sun Y, Xu F, Yang H, Li Z (2009) J Phys Chem C 113:16766
42. Zhou Z-Y, Wang Q, Lin J-L, Tian N, Sun S-G (2010) Electrochim Acta 55:7995
43. Chen W, Kim J, Sun S, Chen S (2007) Langmuir 23:11303
44. Bambagioni V, Bianchini C, Marchionni A, Filippi J, Vizza F, Teddy J, Serp P, Zhiani M (2009) J Power Sources 190:241
45. Su L, Jia W, Schempf A, Ding Y, Lei Y (2009) J Phys Chem C 113:16174
46. Jingyu S, Jianshu H, Yanxia C, Xiaogang Z (2007) Int J Electrochem Sci. 2:64

47. Wang D, Liu J, Wu Z, Zhang J, Su Y, Liu Z, Xu C (2009) Int J Electrochem Sci. 4:1672
48. Zhou WP, Lewera A, Larsen R, Masel RI, Bagus PS, Wieckowski A (2006) J Phys Chem B 110:13393
49. Winjobi O, Zhang Z, Liang C, Li W (2010) Electrochim Acta 55:4217
50. Tarnowski DJ, Korzeniewski C (1997) J Phys Chem B 101:253
51. Li Z, Gao J, Xing X, Wu S, Shuang S, Dong C, Paau MC, Choi MMF (2010) J Phys Chem C 114:723
52. Bard AJ, Faulker LR (1984) Electrochemical methods. Chemical Industry Press, Beijing